iScience, Volume *24*

Supplemental Information

Neural signaling modulates metabolism of gastric cancer

Hanne-Line Rabben, Gøran Troseth Andersen, Magnus Kringstad Olsen, Anders Øverby, Aleksandr Ianevski, Denis Kainov, Timothy Cragin Wang, Steinar Lundgren, Jon Erik Grønbech, Duan Chen, and Chun-Mei Zhao

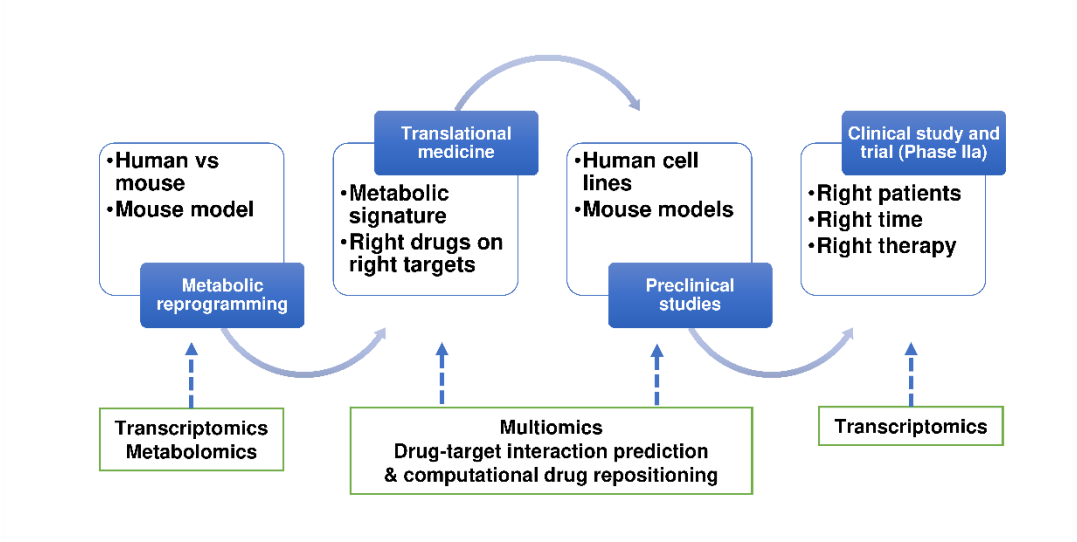

Figure S1, Study design, related to Figure 1: Drawing showing study design of translational research approach and methodology used (indicated in arrows).

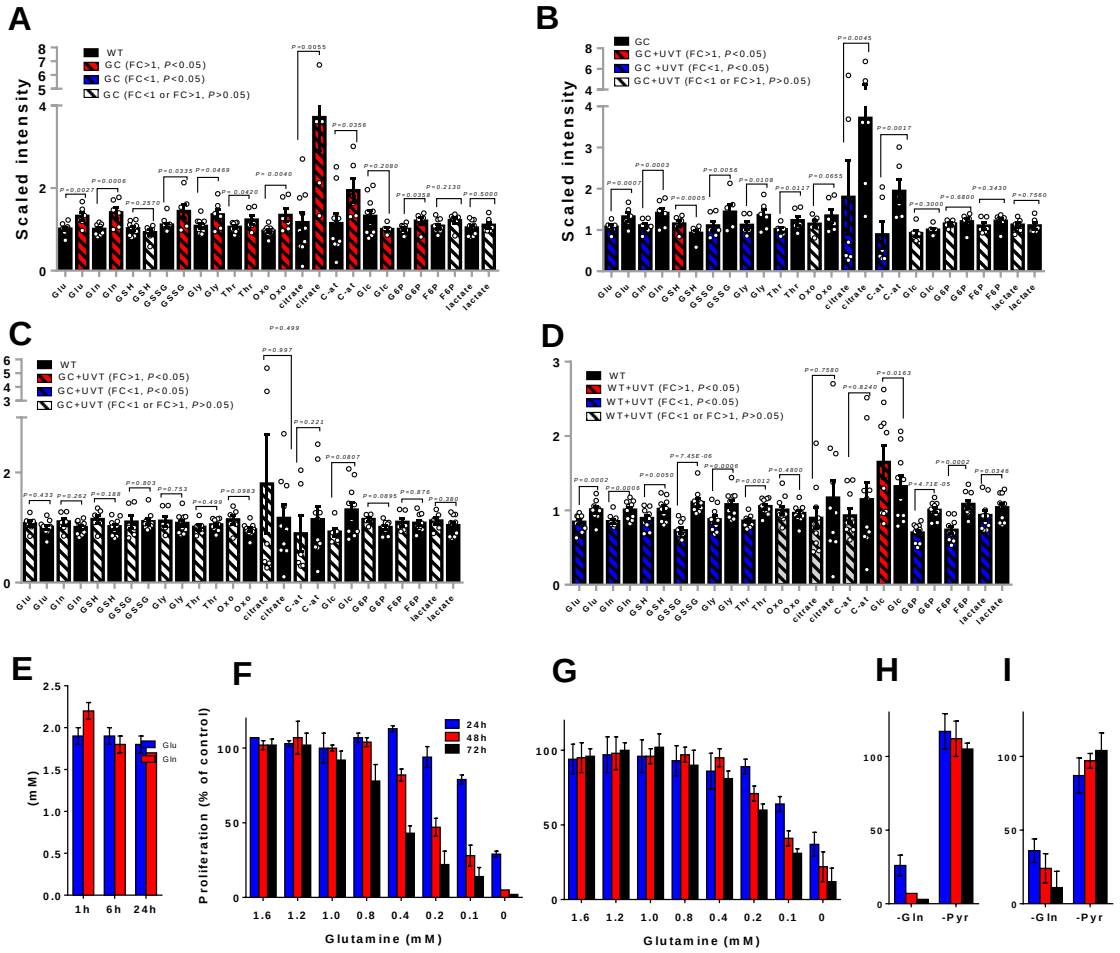

Figure S2, Gastric cancer is glutamine-dependent, related to Figure 4: Levels of metabolites in mouse gastric cancer (GC) (marked in black), wild-type WT (blue), GC after vagotomy (VT) (red) and WT after vagotomy (VT) (purple)(**A-D**) related to **Figure 4.** Glu: L-glutamate; Gln: L-glutamine; GSH: reduced glutathione; GSSG: oxidized glutathione; Gly: glycine; Thr: threonine; Oxo: 5-oxoproline; C-at: cis-aconitate; Glc: glucose; G6P: glucose-6-phosphate; F6P: fructose-6-phosphate. Bars represent relative scaled intensities with SEM and one-way ANOVA p-values. The values were as same as ones in **Figure. 4B-N.** For detailed information, see Table S6. Endogenous levels of L-glutamate and L-glutamine in gastric cancer cells AGS during culture period from 1 to 24 hrs (**E**). Gln reduction (**F,G**) and Gln or Pyr depletion (**H,I**) in the medium in AGS (**F,H**) and MKN45 (**G,I**) cell culture periods of 24, 48 and 72 hrs. Mean of n=3-12 replicates/treatment with SD. Proliferation was assessed using Cell count reagent SF and cell proliferation was calculated relative to controls.

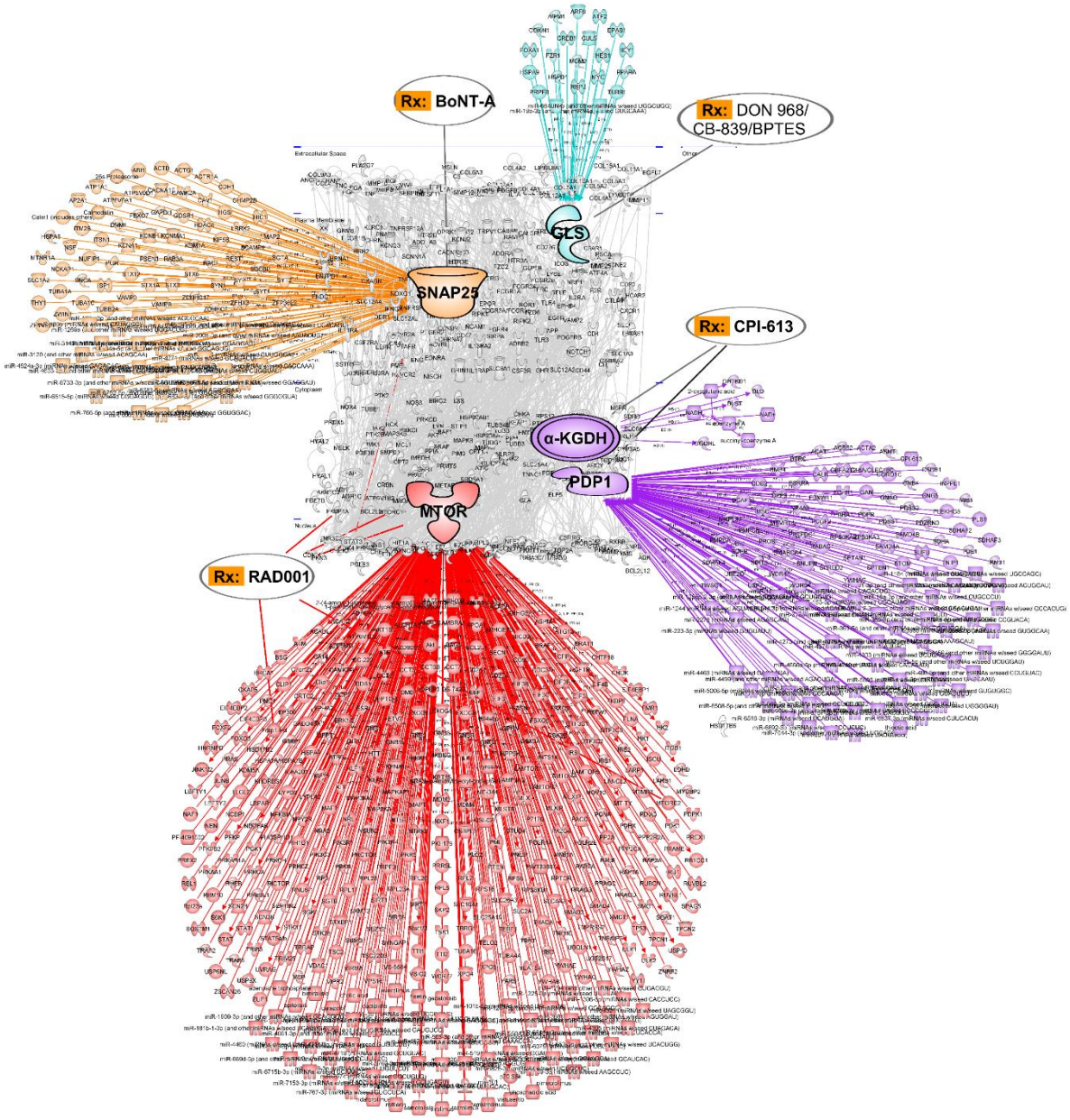

Figure S3, Drug target prediction, related to Figure 6: Waterdrop diagrams showing drug-target interaction prediction and computational drug repositioning in human GC. Note: nodes of RAD001-targeted mTOR (marked in red), CPI-613-targeted PDP1 and α-KGDH (also known as OGDH, purple), BoNT-A-targeted SNAP25 (yellow) and L-DON/968/CB-839/BPTES-targeted GLS (light blue). Lines represent biological interactions between molecules that include proteins, genes, mRNAs, microRNA, lncRNAs and metabolites, generated from differentially expressed drug target genes (only drug targets differentially expressed at $p<0.05$, $q<0.05$ are shown).

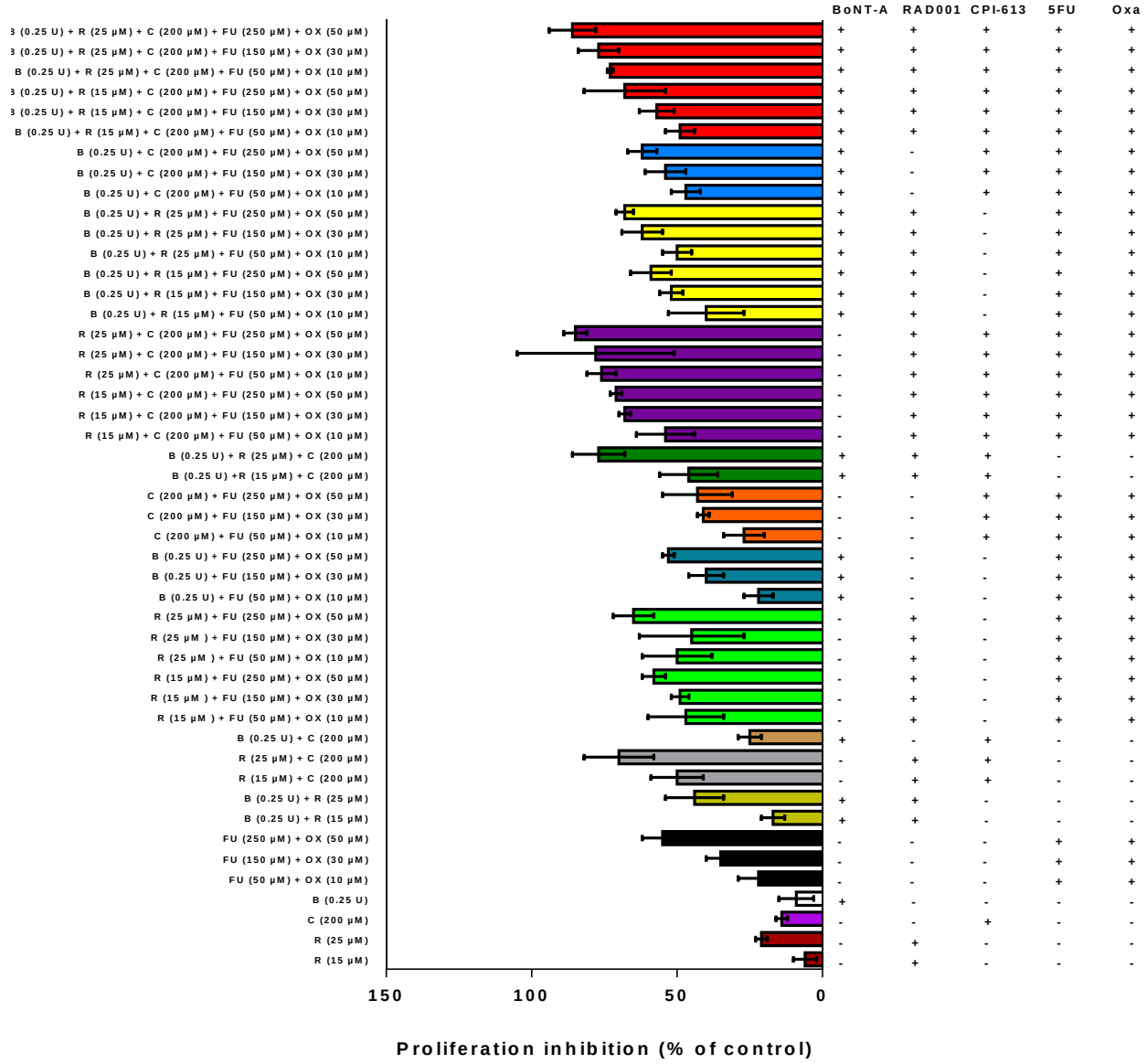

Figure S4, *In vitro* drug screening, related to Figure 7: Proliferation inhibition rates of *in vitro* treatment of BoNT-A, RAD001, CPI-613, 5-FU and oxaliplatin either alone or in different combinations at increasing doses using MKN74 cells. Mean of n=3-12 replicates/treatment with SD. Proliferation was measured using CCK-8 Kit at 450 nm and treatments were normalized to respective vehicle controls.

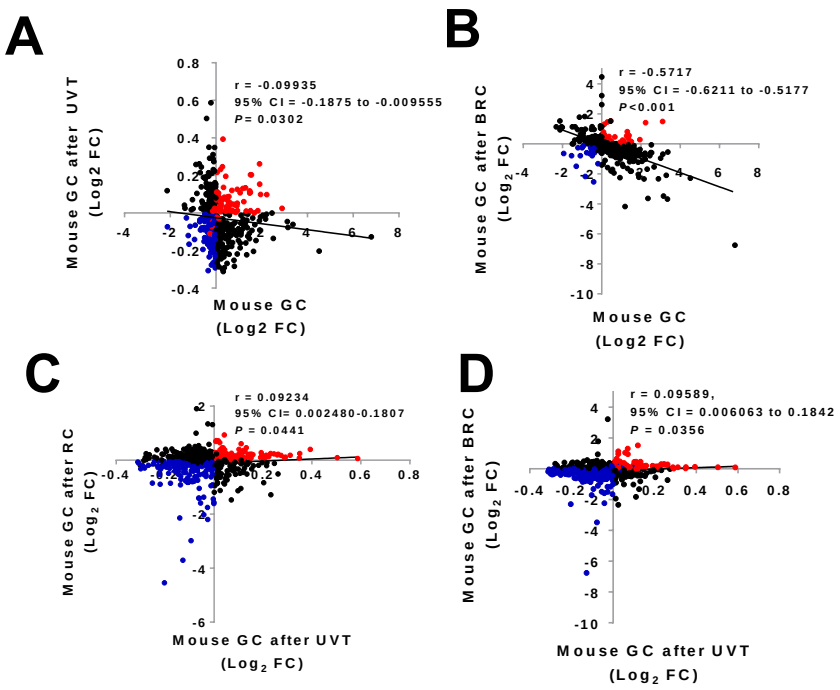

Figure S5, Nerve-cancer metabolism in gastric cancer, related to Figure 8A: Transcriptome profiling of genes involved in the nerve-cancer metabolism pathways of synaptogenesis signaling pathway, WNT/β-catenin signaling, mTOR pathway and energy metabolism. Correlations between mouse GC with *vs.* without unilateral vagotomy (UVT)(**A**), between mouse GC with *vs.* without BRC (**B**), between mouse GC with RC *vs.* UVT (**C**), and between mouse GC with BRC *vs.* UVT (**D**). Linear regression lines were drawn using GraphPad Prism v6. Pearson's test for correlation was used.

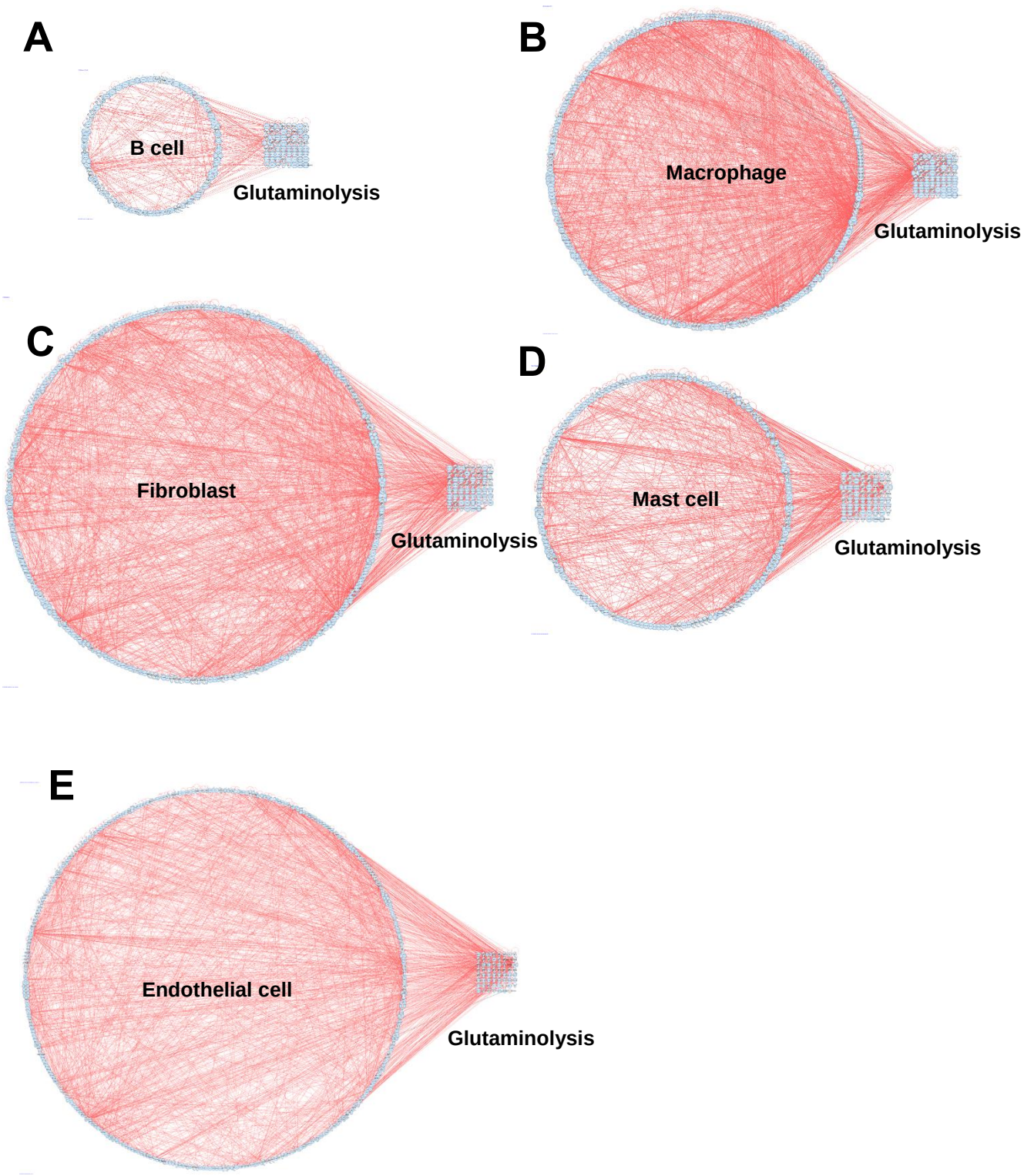

Figure S6, Single-cell atlas and glutamine pathways, related to Figure 8C-D: Computational network modeling showing interactions within B cell gene markers (**A**), macrophage gene markers (**B**), fibroblast gene markers (**C**), mast cell gene markers (**D**) and endothelial cell gene markers (**E**) and connections between the cell types and glutaminolysis (**A-E**) based the single-cell transcriptome atlas (Zhang et al., 2019)(GSE134520).

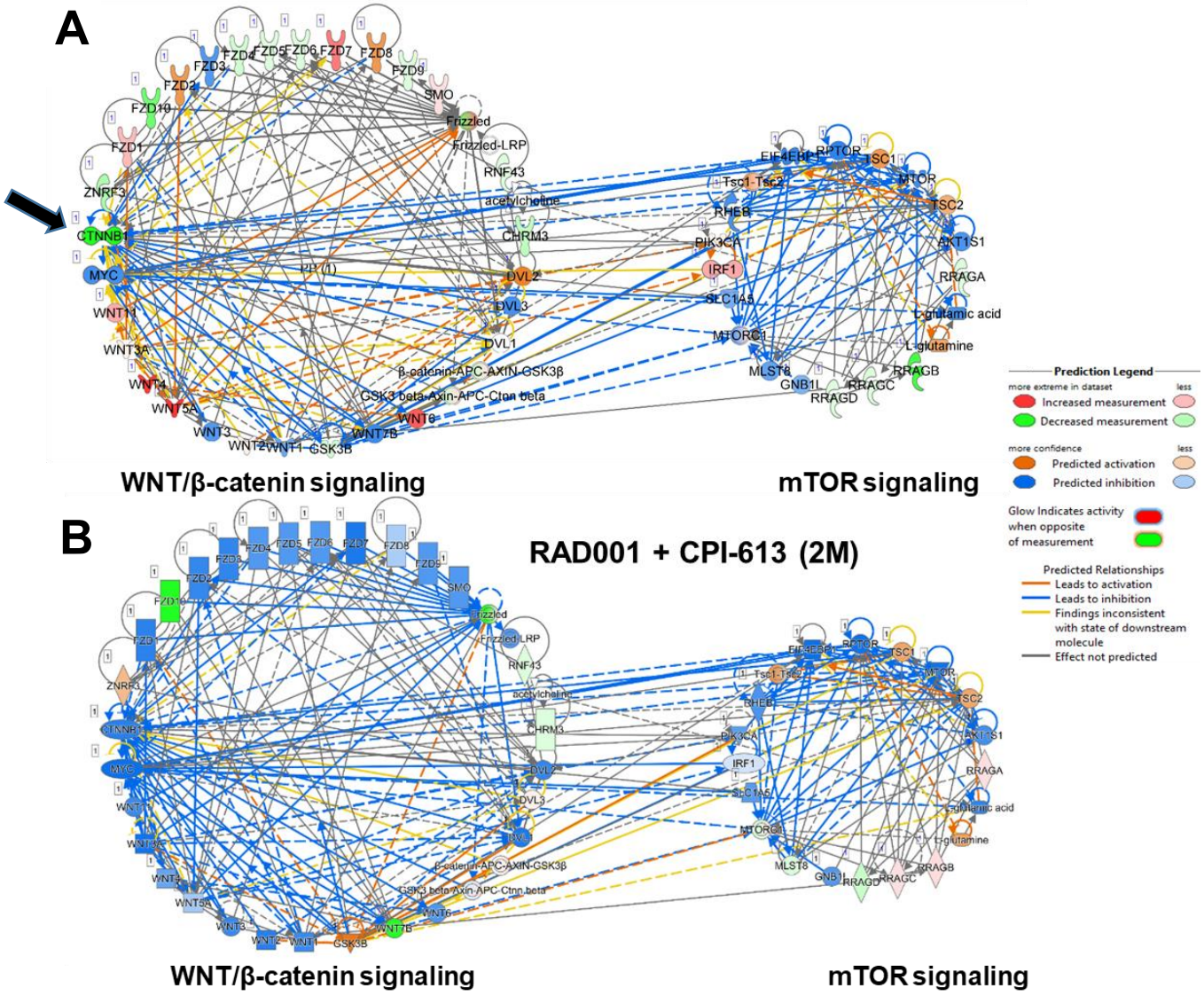

Figure S7, *In silico* modelling, related to Figure 8: Representative prediction of downstream effect of *in silico* inhibition of the CTNNB1 node (marked in green and annotated by black arrow) in the WNT signaling cluster (left) on mTOR signaling (right)(**A**) and effects of treatment of RC for 2 months (2M) on WNT/β-catenin signaling pathway and mTOR signaling clusters (**B**). Overlay gene expression: GC *vs.* WT. MAP (molecular activity prediction) to generate predictions. Semi-quantitative method: dark blue represent -2, light blue represent -1, white represent 0, light orange represent +1 and dark orange represent +2.

Table S1, Genes detected by real-time PCR and RNAseq, related to Figure 1: List of genes detected by both RNAseq and real-time PCR and correlation analysis (figure).

	GenBank	Gene		GenBank	Gene
1	**NM_010347**	Aes	54	**NM_133955**	Rhou
2	**NM_007462**	Apc	55	**NM_029457**	Senp2
3	**NM_009733**	Axin1	56	**NM_013834**	Sfrp1
4	**NM_029933**	Bcl9	57	**NM_009144**	Sfrp2
5	**NM_009771**	Btrc	58	**NM_016687**	Sfrp4
6	**NM_023465**	Ctnnbip1	59	**NM_012030**	Slc9a3r1
7	**NM_007631**	Ccnd1	60	**NM_011441**	Sox17
8	**NM_009829**	Ccnd2	61	**NM_009309**	T
9	**NM_007632**	Ccnd3	62	**NM_009332**	Tcf3
10	**NM_146087**	Csnk1a1	63	**NM_009331**	Tcf7
11	**NM_139059**	Csnk1d	64	**NM_011599**	Tle1
12	**NM_007788**	Csnk2a1	65	**NM_019725**	Tle2
13	**NM_013502**	Ctbp1	66	**NM_011915**	Wif1
14	**NM_009980**	Ctbp2	67	**NM_018865**	Wisp1
15	**NM_007614**	Ctnnb1	68	**NM_021279**	Wnt1
16	**NM_172464**	Daam1	69	**NM_009518**	Wnt10a
17	**NM_178118**	Dixdc1	70	**NM_009519**	Wnt11
18	**NM_010051**	Dkk1	71	**NM_053116**	Wnt16
19	**NM_010091**	Dvl1	72	**NM_023653**	Wnt2
20	**NM_007888**	Dvl2	73	**NM_009520**	Wnt2b
21	**NM_177821**	Ep300	74	**NM_009521**	Wnt3
22	**NM_134015**	Fbxw11	75	**NM_009522**	Wnt3a
23	**NM_013890**	Fbxw2	76	**NM_009523**	Wnt4
24	**NM_013907**	Fbxw4	77	**NM_009524**	Wnt5a
25	**NM_010202**	Fgf4	78	**NM_009525**	Wnt5b
26	**NM_010235**	Fosl1	79	**NM_009526**	Wnt6
27	**NM_008238**	Foxn1	80	**NM_009527**	Wnt7a
28	**NM_008043**	Frat1	81	**NM_009528**	Wnt7b
29	**NM_011356**	Frzb	82	**NM_009290**	Wnt8a
30	**NM_008045**	Fshb	83	**NM_011720**	Wnt8b
31	**NM_021457**	Fzd1	84	**NM_139298**	Wnt9a
32	**NM_020510**	Fzd2	85	**NM_010368**	Gusb
33	**NM_021458**	Fzd3	86	**NM_013556**	Hprt1
34	**NM_008055**	Fzd4	87	**NM_008302**	Hsp90ab1
35	**NM_022721**	Fzd5	88	**NM_008084**	Gapdh
36	**NM_008056**	Fzd6	89	**NM_007393**	Actb
37	**NM_008057**	Fzd7	90	**SA_00106**	MGDC
38	**NM_008058**	Fzd8	91	**SA_00104**	RTC
39	**NM_019827**	Gsk3b	92	**SA_00104**	RTC
40	**NM_010591**	Jun	93	**SA_00104**	RTC
41	**NM_032396**	Kremen1	94	**SA_00103**	PPC
42	**NM_010703**	Lef1	95	**SA_00103**	PPC
43	**NM_008513**	Lrp5	96	**SA_00103**	PPC
44	**NM_008514**	Lrp6			
45	**NM_010849**	Myc			
46	**NM_027280**	Nkd1			
47	**NM_008702**	Nlk			
48	**NM_011098**	Pitx2			
49	**NM_023638**	Porcn			
50	**NM_019411**	Ppp2ca			
51	**NM_016891**	Ppp2r1a			
52	**NM_009358**	Ppp2r5d			
53	**XM_134865**	Pygo1			

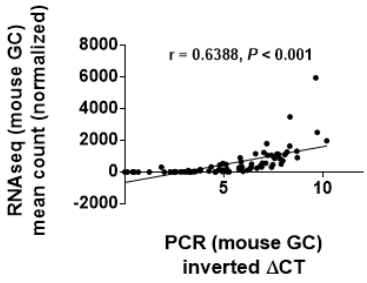

Table S2, Upstream regulators in mouse GC, related to Figure 2F: Upstream analysis of WNT/β-catenin pathway regulators and mTOR targets in mouse GC, related to **Figure 2F.** Predicted Activation State was Activated for z-score>2.000.

Upstream Regulator	Log_2 FC	Predicted Activation State	Activation z-score	p-value of overlap	Target Molecules in Dataset	Target molecules in mTOR pathway	Molecules
Tgf beta		Activated	3.848	2.99E-07	65	0	
WNT1	0.000	Activated	3.138	6.85E-03	34	3	EIF3C,MRAS,PDPK1
CD44	1.156	Activated	3.695	6.05E-08	55	0	
JUN	0.184	Activated	2.219	5.21E-03	55	1	RHOB
TGFB1	0.727	Activated	5.957	2.39E-17	236	3	PPP2CA,PRKCG,RHOA
TGFBR1	-0.536	Activated	2.735	5.98E-04	20	0	
TGFB2	1.573	Activated	3.309	4.55E-11	34	0	
CTNNB1	0.208	Activated	3.741	4.53E-10	165	1	PPP2CA

Table S3, Metabolite signature, related to Figure 4: List of metabolites of gastric cancer (GC) mice and wild-type (WT) mice presented in **Figure 4A.** *GC: gastric cancer; WT: wild-type; FC: Fold change.* Green: p≤0.05, fold change <1.00; Red: p≤ 0.05, fold change ≥1.0. White: p<0.05, 1.0 ≤ fold change >1.0.

Metabolite	Mouse GC *vs.* WT (FC)	Mouse GC after vagotomy *vs.* GC (FC)	Mouse GC after vagotomy *vs.* WT (FC)	Mouse WT after vagotomy *vs.* WT (FC)
prostaglandin B2	4.92	0.54	2.63	0.94
1-arachidonoyl-2-hydroxy-sn-glycero-3-phosphoethanolamine	2.64	0.52	1.36	0.64
inositol 1-phosphate	1.46	0.78	1.14	0.80
docosahexaenoic acid	0.75	1.32	1.00	1.16
gamma-butyrobetaine	0.74	1.22	0.90	1.14
8Z,11Z,14Z-eicosatrienoic acid	0.74	1.45	1.08	0.87
adrenic acid	0.71	1.34	0.95	0.90
13,16-docosadienoic acid	0.65	1.35	0.87	1.06
phosphorylcholine	0.64	1.17	0.75	0.95
propionyl-L-carnitine	0.63	1.71	1.07	1.35
sn-glycero-3-phosphocholine	0.60	1.48	0.89	1.02
arachidonic acid	0.59	1.51	0.88	0.97
icosapent	0.54	1.84	0.99	0.95
1-stearoyl-2-hydroxy-sn-glycero-3-phosphoethanolamine	0.53	1.48	0.79	0.85
cis-4,7,10,13,16-docosapentaenoic acid	0.52	1.64	0.85	1.02
eicosa-11Z, 14Z-dienoic acid	0.51	1.59	0.82	1.01
rac-1-stearoylglycerol	0.47	1.83	0.87	1.09
sn-glycerol-3-phosphate	0.46	1.49	0.69	1.08
3-dehydrocarnitine	0.45	1.11	0.50	0.96
1-palmitoyl-2-hydroxy-sn-glycero-3-phosphoethanolamine	0.44	1.79	0.78	0.91
1-oleoyl-lysophosphatidylethanolamine	0.39	1.82	0.71	0.84
D-sphingosine	0.35	1.87	0.66	0.90
oleoylcarnitine	0.32	2.19	0.71	1.22
citric acid	3.18	0.48	1.54	0.77
cis-aconitic acid	1.70	0.46	0.78	0.81
N-acetyl-L-methionine	2.08	0.59	1.22	0.63
S-glutathionyl-L-cysteine	1.56	0.64	1.00	0.79
L-glutamine	1.40	0.78	1.10	0.85
L-glutamic acid	1.31	0.81	1.06	0.84
glutathione disulfide	1.30	0.77	0.99	0.66
glycine	1.26	0.83	1.04	0.81
L-threonine	1.17	0.82	0.96	0.82
betaine	0.75	1.14	0.86	1.15
5-hydroxytryptamine	0.63	1.36	0.86	1.08
histamine	0.59	1.38	0.81	1.02
gamma-glutamylglutamate	2.15	0.55	1.18	0.83
glycylleucine	1.51	0.82	1.24	0.94
gamma-glutamyl-leucine	1.38	0.76	1.05	1.00
inosine	0.72	1.44	1.03	1.14

deoxyinosine	**0.56**	**1.80**	1.00	**1.63**
guanosine	**0.52**	**1.81**	0.93	**1.55**
deoxyguanosine	**0.46**	**2.36**	1.08	**1.70**
4'-phosphopantetheine	**0.69**	**1.24**	0.86	**0.84**
5-methyltetrahydrofolic acid	**0.68**	**1.73**	1.18	**1.45**
coenzyme A	**0.55**	**1.54**	0.85	0.84
dephospho-coenzyme A	**0.54**	**2.30**	1.25	1.16
beta-glycerophosphoric acid	**0.56**	**1.58**	0.88	1.18
hippuric acid	**0.21**	**1.41**	0.30	**1.25**

Table S4, Energy metabolites, related to Figure 4B-N: Statistic data corresponding to metabolites shown in **Figure 4B-N and Figure S2A-D.**

	WT	***WT (+UVT)***	***GC***	***GC (+UVT)***	***WT v GC***	***GC (+UVT) v GC***	***GC (+)UVT v WT***	***WT (+UVT) v WT***
	Mean ± SEM	**Mean** ± SEM	**Mean** ± SEM	**Mean** ± SEM	***p*-value**	***p*-value**	***p*-value**	***p*-value**
Glu	**1.0058** ±0.041	**0.8414** ±0.0345	**1.3163** ±0.0995	**1.0686** ±0.0582	2.70E-03	7.00E-04	4.33E-01	2.00E-04
Gln	**1.0034**±0.0389	**0.8494** ±0.0263	**1.4036** ±0.1324	**1.1014** ±0.0692	6.00E-04	3.00E-04	2.62E-01	6.00E-04
GSH	**1.0143**±0.0482	**0.8903** ±0.0427	**0.9225** ±0.0757	**1.1482** ±0.0755	2.57E-01	5.00E-04	1.88E-01	5.00E-03
GSSG	**1.1073**±0.0499	**0.7275** ±0.0381	**1.436** ±0.1722	**1.0995** ±0.1168	3.35E-02	5.60E-03	8.03E-01	7.45E-06
Gly	**1.0762**±0.0582	**0.8745** ±0.0509	**1.3519** ±0.1394	**1.1159** ±0.0929	4.69E-02	1.08E-02	7.53E-01	6.00E-04
Thr	**1.0502**±0.0332	**0.8572** ±0.0248	**1.2261** ±0.1052	**1.0057** ±0.0528	4.20E-02	1.17E-02	4.99E-01	1.20E-03
Oxo	**0.9594**±0.0373	**1.0037** ±0.0543	**1.3394** ±0.1572	**1.1404** ±0.0842	4.00E-03	6.55E-02	9.83E-02	0.48E-01
citrate	**1.1665**±0.2424	**0.8943** ±0.1402	**3.7086** ±0.787	**1.7935** ±0.8935	5.50E-03	4.50E-03	9.97E-01	7.58E-01
C-at	**1.1432**±0.2318	**0.9253** ±0.0949	**1.9406** ±0.2825	**0.8868** ±0.3289	3.56E-02	1.70E-03	2.21E-01	8.24E-01
Glc	**1.3181**±0.1462	**1.6463** ±0.2223	**0.9975** ±0.0467	**0.9161** ±0.0768	2.08E-01	3.00E-01	8.07E-02	1.63E-02
G6P	**1.0018**±0.0352	**0.6972** ±0.039	**1.2008** ±0.084	**1.1456** ±0.0344	3.58E-02	6.80E-01	8.95E-02	4.71E-05
F6P	**1.0808**±0.0486	**0.7342** ±0.0466	**1.213** ±0.0772	**1.0979** ±0.0733	2.13E-01	3.43E-01	8.76E-01	2.00E-04
lactate	**1.0359**±0.058	**0.9311** ±0.0669	**1.1007** ±0.0744	**1.1203** ±0.0641	5.00E-01	7.56E-01	3.80E-01	3.46E-02

Mean: scaled intensity of N=10 (WT) or N=6 (GC), *p*-value: One-way ANOVA test between groups, GC: Gastric cancer, WT: wild-type, UVT: Unilateral vagotomy, Glu: L-glutamate, Gln: L-glutamine, GSH: glutathione, reduced, GSSG: glutathione, oxidized, Gly: glycine, Thr: threonine, Oxo: 5-oxoproline, C-at: cis-aconitate, Glc: glucose, G6P: fructose-6-phosphate, F6P: fructose-6-phosphate.

Table S5, Signaling pathways involved in mouse gastric cancer (GC), related to Figure 5A: Multi-omics integrative analysis in IPA revealed 41 signaling pathways that appeared exclusively in Mouse GC *vs*. WT.

Common signaling pathway (IPA)	**Transcriptomics**		**Metabolomics**	
	-log$_{10}$(*P*)	**Z-score**	**-log$_{10}$(*P*)**	**Z-score**
Ethanol Degradation II	1.49E00	-0.632	3.46E-01	N/A
Acyl Carrier Protein Metabolism	7.12E-01	N/A	2.17E00	N/A
β-alanine Degradation I	4.55E-01	N/A	2.29E00	N/A
Glycine Degradation (Creatine Biosynthesis)	4.55E-01	N/A	1.38E00	N/A
Granulocyte Adhesion and Diapedesis	5.38E00	N/A	1.31E00	N/A
Leucine Degradation I	2.00E00	-1.890	7.03E-01	N/A
Synaptogenesis Signaling Pathway	1.79E00	2.887	4.83E-01	N/A
L-cysteine Degradation III	3.21E-01	N/A	1.38E00	N/A
Sphingosine-1-phosphate Signaling	2.20E00	-0.343	7.42E-01	N/A
Role of MAPK Signaling in the Pathogenesis of Influenza	1.35E00	N/A	8.57E-01	N/A
Glutamate Receptor Signaling	2.68E-01	2.000	2.47E00	N/A
Colorectal Cancer Metastasis Signaling	2.71E00	2.689	6.58E-01	N/A
Oleate Biosynthesis II (Animals)	2.00E00	-0.816	1.51E00	N/A
Aspartate Degradation II	3.89E-01	N/A	1.38E00	N/A
UDP-N-acetyl-D-glucosamine Biosynthesis II	1.04E00	N/A	1.86E00	N/A
Isoleucine Degradation I	2.00E00	-1.890	1.48E00	N/A
Glutamate Degradation II	3.21E-01	N/A	1.51E00	N/A
Valine Degradation I	3.92E00	-2.714	1.34E00	N/A
FXR/RXR Activation	9.43E-01	N/A	1.86E00	N/A
Endocannabinoid Neuronal Synapse Pathway	7.12E-01	1.890	1.57E00	N/A
Taurine Biosynthesis	4.55E-01	N/A	1.51E00	N/A

Fatty Acid β-oxidation I	2.37E-01	N/A	3.21E-01	N/A
Serotonin Degradation	1.78E00	-1.886	1.34E00	N/A
Acetyl-CoA Biosynthesis I (Pyruvate Dehydrogenase Complex)	1.82E00	-2.000	6.58E-01	N/A
Neuroinflammation Signaling Pathway	2.49E00	3.250	7.88E-01	N/A
Prostanoid Biosynthesis	1.76E00	0.447	1.51E00	N/A
Human Embryonic Stem Cell Pluripotency	3.32E00	N/A	6.58E-01	N/A
Trna Splicing	2.22E00	0.775	5.30E-01	N/A
Adenine and Adenosine Salvage III	4.80E-01	N/A	1.99E00	N/A
Purine Ribonucleosides Degradation to Ribose-1-phosphate	4.80E-01	N/A	2.72E00	N/A
Glutathione Biosynthesis	3.21E-01	N/A	2.29E00	N/A
Ethanol Degradation IV	2.14E00	0.000	3.75E-01	N/A
Fcγ Receptor-mediated Phagocytosis in Macrophages and Monocytes	2.41E00	1.890	5.88E-01	N/A
Phospholipase C Signaling	3.39E00	0.832	4.83E-01	N/A
Eicosanoid Signaling	2.02E00	0.905	1.27E00	N/A
Branched-chain α-keto acid Dehydrogenase Complex	1.60E00	N/A	6.58E-01	N/A
Purine Nucleotides Degradation II (Aerobic)	3.23E-01	2.000	1.34E00	N/A
Endothelin-1 Signaling	2.14E00	1.820	2.78E-01	N/A
L-cysteine Degradation I	7.64E-01	N/A	1.38E00	N/A
2-oxobutanoate Degradation I	2.22E00	-2.000	3.46E-01	N/A
Flavin Biosynthesis IV (Mammalian)	4.55E-01	N/A	1.51E00	N/A

Table S6, Signaling pathways involved in mouse gastric cancer (GC) after vagotomy, related to Figure 5B: Multi-omics integrative analysis in IPA revealed 24 signaling pathways that appeared exclusively in mouse GC after vagotomy *vs.* sham operation.

Common signaling pathway (IPA)	**Transcriptomics**		**Metabolomics**	
	-log$_{10}$(*P*)	**Z-score**	**-log$_{10}$(*P*)**	**Z-score**
Vitamin-C Transport	2.60E-01	N/A	1.88E00	N/A
Phosphatidylcholine Biosynthesis I	7.01E-01	N/A	1.57E00	N/A
CDP-diacylglycerol Biosynthesis I	2.17E+00	-0.707	1.49E00	N/A
Synaptic Long Term Depression	4.92E-01	-1.706	1.66E00	N/A
Coenzyme A Biosynthesis	4.99E-01	N/A	2.61E00	N/A
Superpathway of Serine and Glycine Biosynthesis I	1.39E00	N/A	1.42E00	N/A
Gαq Signaling	1.89E+00	-1.961	7.14E-01	N/A
Amyotrophic Lateral Sclerosis Signaling	2.25E00	-0.626	1.66E00	N/A
Tetrapyrrole Biosynthesis II	9.55E-01	N/A	1.76E00	N/A
tRNA Charging	7.93E-01	-1.134	1.61E00	2.000
Pyrimidine Ribonucleotides Interconversion	4.13E-01	-2.449	1.49E00	N/A
Purine Nucleotides De Novo Biosynthesis II	2.22E00	0.447	1.37E00	N/A
Phosphatidylglycerol Biosynthesis II (Non-plastidic)	1.95E00	-0.707	1.24E00	N/A
Serine Biosynthesis	1.85E00	N/A	6.7E-01	N/A
5-aminoimidazole Ribonucleotide Biosynthesis I	1.41E00	N/A	2.2E00	N/A
Glutathione Redox Reactions I	3.64E-01	N/A	1.88E00	N/A
Adipogenesis pathway	4.18E-01	N/A	1.58E00	N/A
Stearate Biosynthesis I (Animals)	1.50E00	-1.897	5.04E-01	N/A
Arsenate Detoxification I (Glutaredoxin)	3.99E-01	N/A	1.42E00	N/A
Serotonin and Melatonin Biosynthesis	3.28E-01	N/A	1.49E00	N/A
Triacylglycerol Biosynthesis	1.14E00	-1.000	1.42E00	N/A
Antioxidant Action of Vitamin C	0.00E00	2.530	2.02E00	N/A
Ascorbate Recycling (Cytosolic)	4.99E-01	N/A	1.76E00	N/A

Ceramide Signaling	1.62E00	-1.414	9.96E-01	N/A

Table S7, Signaling pathways involved in mouse gastric cancer (GC) with and without vagotomy, related to Figure 5C: Multi-omics integrative analysis in IPA revealed 13 signaling pathways present in comparison between mouse GC *vs.* WT and in mouse GC after vagotomy *vs.* sham operation.

Common signaling pathway (IPA)	**Mouse GC *vs.* WT**				**Mouse GC after vagotomy**			
	Transcripts		**Metabolites**		**Transcripts**		**Metabolites**	
	-log$_{10}$(*P*)	**Z-score**	**-log$_{10}$(*P*)**	**Z-score**	**-log$_{10}$(*P*)**	**Z-score**	**-log$_{10}$(*P*)**	**Z-score**
Gap Junction Signaling	2.6E00	N/A	8.93E-01	N/A	6.31E-01	N/A	1.36E00	N/A
Phospholipases	1.71E00	1.886	4.06E-01	N/A	0.00E00	-2.449	1.57E00	N/A
Sirtuin Signaling Pathway	3.17E-01	0.949	1.71E00	N/A	2.34E00	-1.029	6.68E-01	N/A
Protein Kinase A Signaling	1.61E00	-0.232	3.46E-01	N/A	2.45E00	-1.089	5.61E-01	N/A
Asparagine Biosynthesis I	7.12E-01	N/A	1.38E00	N/A	9.24E-01	N/A	1.88E00	N/A
TCA Cycle II (Eukaryotic)	5.51E-01	-2.449	2.91E00	N/A	2.77E-01	N/A	1.97E00	N/A
Choline Biosynthesis III	2.71E00	0.378	4.41E-01	N/A	2.03E00	-1.342	1.66E00	N/A
γ-glutamyl Cycle	3.33E00	0.707	2.58E00	N/A	3.68E-01	N/A	2.39E00	N/A
Leukotriene Biosynthesis	1.77E00	2.449	1.02E00	N/A	1.34E00	-1.000	2.61E00	N/A
Agranulocyte Adhesion and Diapedesis	5.38E00	N/A	1.31E00	N/A	4.78E-01	N/A	1.58E00	N/A
Superpathway of Methionine Degradation	9.67E-01	-2.530	2.31E00	2.236	0.00E00	1.000	1.96E00	-2.000
Calcium Signaling	1.52E00	1.826	1.27E00	N/A	7.62E-01	-2.236	1.76E00	N/A
Glutathione-mediated Detoxification	1.02E00	-0.707	1.75E00	N/A	1.16E00	-1.633	3.75E00	-1.000

Table S8, Baseline patient data, related to Figure 8L: Baseline patient data (the first patient was recruited at September 10,

Patient number	Age at inclusion	TNM stage at time of diagnosis	Chemotherapy	TNM stage at inclusion time	Tumor location and size
1	81	T4N1M1	1st line treatment, stopped due toxic side effects	T4N1M1	Greater curvature, lesser curvature and anterior wall. Longest diameter 9 cm
2	70	T3N0M0	Neoadjuvant chemotherapy, inoperabel due to comorbidity	T3N1M0	Cardia and proximal esophagus. Longest diameter 3 cm
3	79	T4aN2M1	Palliativ chemotherapy with EOX	T4aN2M1	Distal part of the stomach. Circular tumor with longest diameter 8 cm
4	49	TxNxM1	1st line treatment, 2nd line treatment.	TxNxM1	Cardia. Extensive liver metastasis
5	83	TxNxMx	No previous chemotherapy due to age and comorbidity	T4aN3M1	Cardia. Extensive liver metastasis
6	84	T4aN3M0	No previous chemotherapy due to age and comorbidity	T4aN3M0	Linitis plastica in whole stomach except the most proximal part

2014).

Note: One additional patient (i.e. patient no. 7) gave his consent for participation in this study, but pretreatment CT scan of the stomach showed no measurable tumor size. According to the study protocol (Supplementary Data Clinical study protocol), this patient was excluded from further participation in the study and did not receive BoNT-A treatment.

Table S9, Primary outcome measures, related to Figure 8L: Primary outcome measure: Tumor evaluation

Patient number	Tumor thickness, diameter or volume density (mean±SD % before BoNT-A injection	Tumor thickness, diameter or volume density (%) 8 weeks after injection	Tumor diameter and volume density (%) 20 weeks after injection
1	14 mm tumor thickness	Not followed (died before the time point)	Not followed (died before the time point)
2	27 x 16 mm, 20x17 mm, 40.8±10.9 %	32x21 mm and 26x20 mm, 34.4±5.3 %	31x21 mm, 28x21 mm, 27.9±10.8 %
3	17-19 mm tumor thickness	Not followed (died before the time point)	Not followed (died before the time point)
4	20x29 mm	Not followed (died before the time point)	Not followed (died before the time point)
5	12 mm tumor thickness	Not followed (died before the time point)	Not followed (died before the time point)

6	22 mm tumor thickness	26 mm tumor thickness	Not followed ((died before the time point)

Table S10, Secondary outcome measure (short term), related to Figure 8L: Secondary outcome measure: Short-time adverse effects and ECOG status after BoNT-A injections

Patient number	Baseline ECOG	Adverse effects during procedure	Adverse effects after observation 24 hours after procedure	Adverse effects at 2 weeks outpatient clinical control	ECOG after 2 weeks
1	1	No	No	No	1
2	2	No	No	No	2
3	1	No	No	No	2
4	1	No	No	No	3
5	1	No	No	No	ECOG status missing from local hospital
6	2	No	No	No	1

Table S11, Secondary outcome measures (long-term), related to Figure 8L. Secondary outcome measure: Long term adverse effects and ECOG status after BoNT-A injections

Patient number	Survival days after BoNT-A injection	8 weeks (56 days) outpatient control performed	Adverse effects /ECOG status	20 weeks control performed	Adverse effects /ECOG status	Any adverse events during the course of the disease until death
1	51	Died before control				Death related to natural progression of disease and no adverse effects recorded until time of death.
2	188	Yes	No/3	Yes	No/3	Death related to natural progression of disease and no adverse effects recorded until time of death.
3	69	Withdrawal from study protocol due to severe progression of disease				Death related to natural progression of disease and no adverse effects recorded until time of death.
4	37	Died before control				Death related to natural progression of disease and no adverse effects recorded until time of death.
5	27	Died before control				Death related to natural progression of disease and no adverse effects recorded until time of death.
6	112	Yes	No/1	No		Death related to natural progression of disease and no adverse effects recorded until time of death.

Table S12, Study groups, related to Figure 7K and Figure 8G-L.

Group	Subjects	Treatment (*N*)(female/male)	Age at intervention	Age at examination
Clinical examination	GC patients	Gastrectomy (16)(6/10)	54-87 years	5 years follow-up
Transcriptomics	**GC mice#**	**UVT (6) (4/2)**	6 months	12 months
Metabolomics	**GC mice**	**UVT (6) (2/4)**	6 months	12 months
		Sham (6)(2/4)	6 months	12 months
	WT mice	**UVT (10)(4/6)**	6 months	12 months
		Sham (10)(4/6)	6 months	12 months
Treatments:	**GC mice**	**UVT + saline (9)(7/2)**	12-14 months	14-16 months
		Sham + saline (9)(7/2)	12-14 months	14-16 months
		UVT + FUOX (16)(10/6)	12-14 months	14-16 months
		Sham + FUOX (16)(10/6)	12-14 months	14-16 months
		Sham + FUOX (16)(10/6)	12-14 months	14-16 months
		Sham + FUOX (16)(10/6)	12-14 months	14-16 months
		BoNT-A + saline (22)(12/10)	12-14 months	14-16 months
		Saline (22)(12/10)	12-14 months	14-16 months
		BoNT-A + FU (12)(7/5)	12-14 months	14-16 months
		FU (12)(7/5)	12-14 months	14-16 months
		BoNT-A + OX (26)(14/12)	12-14 months	14-16 months
		OX (26)(14/12)	12-14 months	14-16 months
		BoNT-A + FUOX (26)(15/11)	12-14 months	14-16 months
		FUOX (26)(15/11)	12-14 months	14-16 months
		BoNT-A (10)(5/5)	9-15 months	12-18 months
		Sham (10)(5/5)	9-15 months	12-18 months
		BoNT-A + RAD001 (15)(5/10)	9-15 months	12-18 months
		RAD001 (15)(5/10)	9-15 months	12-18 months
		BoNT-A + RAD001 + FUOX (48)(24/24)	9-15 months	12-18 months
		RAD001 + FUOX (48)(24/24)	9-15 months	12-18 months
		BoNT-A + CPI-613 (8)(5/3)	9-15 months	12-18 months
		CPI-613 (8)(5/3)	9-15 months	12-18 months
		BoNT-A + CPI-613 + FUOX (12)(6/6)	9-15 months	12-18 months
		CPI-613 + FUOX (12)(6/6)	9-15 months	12-18 months
		BoNT-A + RAD001 + CPI-613 (25)(13/12)	9-15 months	12-18 months
		RAD001 + CPI-613 (25)(13/12)	9-15 months	12-18 months
		BoNT-A + RAD001 + CPI-613 + FUOX (31)(15/16)	9-15 months	12-18 months
		RAD001 + CPI-613 + FUOX (31)(15/16)	9-15 months	12-18 months
		Age-matched controls (32)(15/17)	9-15 months	12-18 months
		Age-matched controls (32)(15/17)	9-15 months	12-18 months
Clinical trial	GC patients	Endoscopic injection of BoNT-A (6)	49-84 years	2 years follow-up

 # group from previous study (Zhao et al., 2014)

Table S13. Metabolites involved with DNA/protein synthesis, related to Figure 4 and Data S3. Effects of vagotomy (unilateral vagotomy, UVT) on gastric tissue levels (scaled intensity) of metabolites that are involved in DNA/protein synthesis in either wild-type (WT) or gastric cancer (GC) mice

	WT	**WT (UVT)**	***p*-value**	**GC**	**GC (UVT)**	***p*-value**
	Mean ± SEM	**Mean** ± SEM		**Mean** ± SEM	**Mean** ± SEM	
Choline	**1.0382** ±0.0347	**0.9399** ±0.0421	0.0039	**1.1583** ±0.0950	**1.0341** ±0.0902	0.0179
Creatine	**0.9675** ±0.0329	**0.871** ±0.0323	0.0077	**1.1146** ±0.0439	**1.0931** ±0.0385	0.3415
Cytidine	**1.016** ±0.024	**0.769** ±0.0346	0.0001	**1.2553** ±0.0882	**1.1472** ±0.0387	0.1217
Glycine	**1.0762** ±0.0582	**0.8745** ±0.0509	0.0006	**1.3519** ±0.1394	**1.1159** ±0.0929	0.0054
Histidine	**0.9938** ±0.0471	**0.8598** ±0.0725	0.0035	**1.115** ±0.0848	**1.0622** ±0.0791	0.2282
Sarcosine	**1.0912** ±0.0896	**0.8637** ±0.0898	0.0031	**1.1428** ±0.0949	**0.9587** ±0.1357	0.0182
Serine	**1.0827** ±0.0352	**0.914** ±0.0451	0.0022	**1.0947** ±0.0744	**0.9801** ±0.0546	0.0499
Threonine	**1.0502** ±0.0332	**0.8572** ±0.0248	0.0012	**1.2261** ±0.1052	**1.0057** ±0.0528	0.0059
Uracil	**1.0101** ±0.0383	**0.8603** ±0.0359	0.0015	**1.0947** ±0.0694	**1.0704** ±0.0292	0.3945

One-way ANOVA was used for comparisons between WT and WT (UVT) or between GC and GC (UVT).

Table S14, Chemical and reagent list, related to methods. List of reagents and chemicals used.

Name	Cat. no	Supplier	Country
DMSO	D8418	Sigma-Aldrich	Oslo, Norway
Cell Counting Kit-8 (CCK-8)	96992-3000TESTS-F	Sigma-Aldrich	St. Luis, MO, USA
Cell Count Reagent SF	07553-44	Nacalai tesque	Tokyo, Japan
DMEM (no glucose, no glutamine,, no pyruvate, no phenol red)	08456-65/A14430-01-500ML	Nacalai tesque/Gibco by Life Technologies	Tokyo, Japan/Grand Island, NY
DMEM	A14430-01-500ML		
RPMI-1640 with L-Gln (0.3 g/L, 2.0 mM), phenol red	R8758-500ML	Sigma-Aldrich	Norway
D-glucose			
FBS	F7524	Sigma-Aldrich	Norway
Dialyzed FBS	26400-036	Gibco by Life Technologies	USA
L-Gln	G7513-100ML	Sigma Aldrich	Norway
Glutamine/glutamate detection kit	GLN-1	Sigma-Aldrich	Saint Louis, Missouri, USA
Glutamic Dehydrogenase (L-GLDH)	G5900	Sigma-Aldrich	Saint Louis, Missouri, USA
Glutaminase	G8880	Sigma-Aldrich	Saint Louis, Missouri, USA
NAD	N9268	Sigma-Aldrich	Saint Louis, Missouri, USA
Acetate buffer, 0.5 M, pH 5	A4433	Sigma-Aldrich	Saint Louis, Missouri, USA
Adenosine 5'-Diphosphate (ADP), 100 mM, 1 ml	A4558	Sigma-Aldrich	Saint Louis, Missouri, USA
Hydrazine Hydrate, 3ml	H0883	Sigma-Aldrich	Saint Louis, Missouri, USA
L-glutamine	G6275, 2 mM	Sigma-Aldrich	Saint Louis, Missouri, USA
L-glutamate	G6150, 1 mM	Sigma-Aldrich	Saint Louis, Missouri, USA
RNase A	R4875-100MG	Sigma Aldrich	Oslo, Norway
Propidium Iodide	P4170-10MG	Sigma Aldrich,	Oslo, Norway
Triton-X	T9284	Sigma Aldrich	Oslo, Norway
Sodium acetate buffer (10 mM, CH3COONa, MW: 82.03, pH 5.2)			
Tris-HCl buffer (1M, NH2C(CH2OH)3; MW: 121.14, pH 8.0).			

Tris-EDTA Buffer	T3161		
PBS	BR0014G	Oxoid	Hampshire, England
D-PBS	14249-24	Nacalai-Tesque	Tokyo, Japan
Trypsin-EDTA	T4049-500ML	Sigma-Aldrich	Oslo, Norway
Penicillin/Streptomycin cocktail	P4333-100ML	Sigma-Aldrich	Norway
Botox ®	100U	Botox Allergan Inc.	Norway
RAD001 (also known as Everolimus)	Trl-eve	InvivoGen	San Diego, CA, USA
CPI-613 (also known as Devimistat)	SML0404-25MG	Sigma-Aldrich	Oslo, Norway
Fluorouracil (5-FU)	50 MG/ML, vnr. 137864	Hospira	Illinois, USA
Oxaliplatin	5 MG/ML, vnr. 137098	Hospira	Illinois, USA
NucleoSpin® RNA	June 2015, Rev. 17	Macherey-Nagel	
Beta-Mercaptoethanol	M3148-100ML	Sigma-Aldrich	Oslo, Norway
Bulk beads (1.4 mm/2.8mm Zirconium oxide beads)	03961-1-103/03961-1-102	Precellys 24, Bertin Technologies	France
Illumina TruSeq Stranded mRNA Library Prep kit	20020594	Illumina	
Sodium Pyruvate 110.00 mg/L, 1.0 mM		Nacalai tesque/Sigma Aldrich	Tokyo, Japan/Oslo, Norway
Isoflurane	Baxter		
Viscotears ® eye gel		Thèa	Berlin, Germany

Table S15, Description of Metabolon QC samples, related to methods.

Type	Description	Purpose
MTRX	Large pool of human plasma maintained by Metabolon that has been characterized extensively.	Assure that all aspects of Metabolon process are operating within specifications.
CMTRX	Pool created by taking a small aliquot from every customer sample.	Assess the effect of a non-plasma matrix on the Metabolon process and distinguish biological variability from process variability.
PRCS	Aliquot of ultra-pure water	Process Blank used to assess the contribution to compound signals from the process.
SOLV	Aliquot of solvents used in extraction.	Solvent blank used to segregate contamination sources in the extraction.
DS	Derivatization Standard	Assess variability of derivatization for GC/MS samples.
IS	Internal Standard	Assess variability and performance of instrument.
RS	Recovery Standard	Assess variability and verify performance of extraction and instrumentation.

Transparent Methods

GC patients

Twenty-two patients (17 men aged 49-87 years and 5 women aged 51-83 years) were included. 16 of 22 patients underwent total/subtotal or distal gastrectomy because of intestinal or diffuse gastric cancer and were followed-up for 5 years since 2012 at St. Olavs Hospital, Trondheim, Norway. The study was approved by the Regional Committees for Medical and Health Research Ethics Central Norway (REK 2012-1029). 6 of 22 patients were enrolled in a clinical trial (see below) (Table S12). Total, subtotal or distal gastrectomy was performed on 16 patients diagnosed with gastric cancer. Biopsies from 4 pre-determined positions in corpus (major and minor curvature), cardia and antrum were collected, and largest diameter of the tumor was decided. Biopsies from adjacent, normal tissue was taken 5-10 cm from the tumor site. TNM status was defined, and samples were classified according to Lauren's classification, (Intestinal, diffuse or mixed/combined type), WHO classification (tubular, papillary, mucinous and poorly cohesive), WHO grading (well, moderately or poorly differentiated), and were reviewed according to the Japanese pathological classification. Samples were assigned gastric histopathology scoring including inflammation, epithelial defects, oxyntic atrophy, epithelial hyperplasia and dysplasia and an overall GHAI score.

Animals

Three hundred-twenty four mice were used and some of the mice were followed- up for more than one year to measure the overall survival rate. The mouse GC model was the transgenic INS-GAS mice which spontaneously develop GC at our own institute (Wang et al., 1996; Zhao et al., 2014) and its wild-type (WT) mice (FVB strain). Mice were housed ~5 mice per cage on wood chip bedding with a 12-hour light/dark cycle in a specific pathogen free environment with room temperature of 22°C and 40-60% relative humidity. Mice including both INS-GAS and WT mice were age-matched and randomized into different experimental groups (Table S12). All animal experiments were approved by The Norwegian Food Safety Authority (Mattilsynet).

Surgery

Vagotomy and BoNT-A injections were performed under isoflurane anesthesia as described previously(Zhao et al., 2014). The success of UVT was confirmed by reduced thickness of gastric mucosa (Zhao et al., 2014) and reduced tissue-levels of metabolites that are involved in DNA/protein synthesis in the denervated side in comparison with the innervated side of stomach (Table S13).

Chemicals and reagents

For details, see chemical and reagent list in Table S14.

Cells and cell culture

GC cell lines included AGS (female, 54 years, Caucasian), MKN74 (male, 37 years, Asian), MKN45 (female, 54 years, Caucasian) and KATO-III (male, 55 years, Asian). AGS cells were kindly provided by Prof. Sasakawa (Tokyo University, Japan). MKN45 cells were kindly provided by Prof. Kamiya (Kyorin University, Japan). MKN74 cells were provided by Prof. T.C Wang and KATO-III cells were purchased from LGC group.

AGS and MKN45 cells were maintained in Dulbecco's Modified Eagle's Medium (DMEM (1.0 g/l Glucose, 10 mM) with L-Gln (584.00 mg/L, 4.0 mM) and Sodium Pyruvate (110.00 mg/L, 1.0 mM)(Nacalai tesque, Japan) supplemented with 10% fetal bovine serum (FBS; ThermoFisher Scientific, Grand Island, NY) and antibiotic-antimycotic solution (1%) containing penicillin, streptomycin and amphotericin B (Nacalai tesque, Japan). MKN74 and KATO-III cells were maintained in RPMI-1640 medium (Sigma Aldrich, Norway) supplemented with fetal bovine serum (10%, FBS), Sodium pyruvate and penicillin streptomycin solution (1%) in a humidified incubator holding 5% CO_2 and 37°C.

In vitro experiments

Gln/pyr depletion

The cells ($1.0x10^4$) were plated (24h) and treated with 0-2.0 mM L-glutamine and 1.0 mM pyruvate in DMEM supplemented with dialyzed bovine serum (10%) and glucose at 25 mM. In depletion testing, either glutamine or pyruvate were omitted from the medium. Proliferation was assessed using Cell Count Reagent SF or Cell counting Kit-8 reagent at 450 nm and cell proliferation was calculated relative to controls. Determination of endogenous L-glutamine and L-glutamate was performed after 1, 6 and 24 hrs in culture using a detection kit (Glutamine/glutamate determination kit, Sigma, Saint Louis, Missouri).

Drug screen

Cells ($2.5x10^3$) were plated (24 hrs) and subjected to individual dose-response drug screens and sequential combination treatment during 3 days in culture. First, cells were treated with either serum-free medium or BoNT-A- without serum at 0.25 U BoNT-A/well and incubated for 24 hrs. CPI-613 and RAD001 were dissolved in DMSO at highest solubility before diluted in the medium. The cells were treated with RAD001, CPI-613, combination of these or vehicle (DMSO) control and incubated for 24 hrs. A combination of 5-FU and oxaliplatin or medium control was added to the cells for 24 hrs. To assess whether the drug combinations acted synergistically, we calculated Bliss synergy scores for RAD001 + CPI-613 combinations using the SynergyFinder web-application (Ianevski et al., 2017). Synergy scores were quantified as an average excess over expected drug combination effect given by the Bliss reference model (Ianevski et al., 2019). Bliss Independence model was used because the two drugs (i.e. RAD001 and CPI-613) act independently in such a manner that neither of them interferes with the other (different sites of action), but each contributes to a common result, i.e. cell proliferation.

In vivo experiments

GC mice were injected BoNT-A through laparoscopic procedure as described earlier (Zhao et al., 2014), treated with RAD001 (1.5 mg/kg/day for 3 weeks, i.p.), CPI-613 (20 mg/kg/week, once weekly for 3 weeks, i.p.), or combination of RAD001 and CPI-613. Saline injection (i.p.) was used as control. The mice were allowed one-week rest after the first cycle of treatment, and then the treatment cycle was repeated once, yielding a total treatment window of 8 weeks (**Figure 7H**). BoNT-A was dissolved in saline containing methylene blue (1.0 %) to visualize the injection. The achieved

concentration of BoNT-A was 0.25 U of BoNT-A/mL. Injection was performed through laparotomy into the serosa layer in the anterior side of stomach. Thus, for a mouse receiving 0.4 mL BoNT-A (0.25 U/mL) the dose corresponded to 0.10 U. 5-Fluorouracil (5-FU) was given i.p. at dose of 25 mg/kg in a volume of 0.5 mL. Oxaliplatin was given i.p. at dose of 5 mg/kg in volume of 0.5 mL. The two drugs were injected on either left or right side of abdomen at same time once weekly for 3 weeks in 2 cycles, starting one week after BoNT-A injection.

Sample collection and preparation

Mouse tissue samples were taken after the animals were killed under deep isoflurane inhalation anesthesia. The anterior and posterior parts of stomachs were collected for histopathological analysis and cryopreservation for transcriptomics of mouse GC in which mice underwent unilateral vagotomy (UVT) at 6 months of age and the stomachs were collected 6 months afterwards, the data from our previous study was re-analyzed (according to 3R principle)(Zhao et al., 2014). For metabolomics, GC and WT mice at 6 months of age underwent the same UVT or sham operation and the stomachs were collected as described previously. Six months after UVT, animals were terminated for sampling, and tissue samples from the denervated anterior stomach and tissue samples from the posterior stomach with intact innervation were analyzed with liquid chromatography/mass spectrometry and gas chromatography/mass spectrometry. Mouse tissue samples were collected for transcriptomics analysis immediately after completing two months BRC-treatment.

Measurement of survival rate, body weight and tumor size

Animals were followed up by daily inspection with scoring sheet, weighing and euthanized according to primary human endpoints. Scoring parameters included severe body weight loss (>25%), stress behavior, abdominal pain or reduced physical activity and was followed in collaboration with the responsible veterinarian at the animal facility. Body weight was measured daily (during treatment) or weekly (during follow up). Tumor volume density (% of glandular area of the stomach occupied by tumor) was measured using point count method described earlier[14].

Pilot clinical trial (phase II)

Six patients were enrolled according to inclusion criteria and written consent (Supplementary Data: Clinical Trial Protocol). Inclusion criteria included 1) patients who received 1st line and 2nd line chemotherapy but no longer respond to such therapy, 2) patients who, due to toxicity of chemotherapy, could not be offered such treatment, 3) patients who, after meticulous information about chemotherapy, still did not want such treatment and 4) patients with performance status (ECOG) 0-2. Patients were elderly and diagnosed with already advanced gastric cancer which precluded surgical resection (Table S12). Exclusion criteria included 1) known allergy to any of the components in Botox®, 2) known peripheral motor neuropathy disease (for example: Amyotrophic Lateral Sclerosis, ALS), or subclinical or clinical deficiency of neuromuscular transmission (for example: Myasthenia Gravis or Eaton-Lambert`s Syndrome), 3) another cancer disease that is not under control, 4) another concomitant treatment for cancer, 5) serious mental illness and 6) performance status (ECOG) 3-4. One patient with TNM status T3N0M0 was rejected for surgery due to comorbidity following a short period with neoadjuvant chemotherapy. At the time of

enrollment into this study, 4 out of 6 patients had metastatic disease, and 2 of these patients had extensive liver metastasis with short expected life expectancy. Extensive tumor masses in the stomach were present in 3 out of 6 patients. The patients were admitted to the hospital shortly after the baseline CT scan, and endoscopic BoNT-A injection was performed under sedation with midazolam. One hundred units with Botox® were diluted into 14 mL saline by the Department for Clinical Studies at St.Olav Hospital's Pharmacy. This amount was divided into 7 doses of 2 mL (14.3 U/dose) that were injected at 4 sites around the tumor and at 3 sites directly into the tumor. Some of the patients had advanced and extensive tumor masses in the stomach and for those patients, injections were concentrated to the area of the stomach with measurable tumor thickness or diameter, omitting the rest of the tumor masses in the stomach. After the endoscopic procedure, the patients were observed in the surgical ward and discharged from hospital the day after the procedure. Primary outcome measures were assessment of tumor size (volume density and/or thickness) in the stomach using standardized CT protocols after 2, 8 and 20 weeks. Two weeks after the injection, the patients had an outpatient clinical visit with complete physical assessment, specially emphasizing on detecting any adverse or toxic events related to the experimental treatment. At 8 and 20 weeks after the injection, another thoracic and abdominal CT scan was performed, together with a follow-up outpatient clinical examination. Secondary outcomes included toxicity (within 2- and 8-weeks post injection) and performance status (ECOG) after 2, 8 and 20 weeks. The safety evaluation was performed based on the CTC (Common Toxicity Criteria) criteria. The study was conducted in accordance with the guidelines for GCP (Good Clinical Practice) and it was approved by the Regional Committee for Medical and Health Research Ethics (2012/1031) and the Norwegian Medicines Agency (2012-002493-31).

Transcriptomics

Total RNA was extracted from harvested stomachs of mice or surgical biopsies of patients. RNA quality and quantity were obtained using NanoDrop One (Thermo Scientific, Norway) and Agilent Bioanalyser. RNA sequencing of human GC samples was performed using Illumina platform as described earlier[14], whereas RNA sequencing of mouse samples was performed using Illumina HiSeqNS500 instrument (NextSeq 500) at 75 bp with paired end (PE) reads using NS500H flowcells with 25 M reads/sample. Paired end forward read length (R1): 81, reverse read length (R2): 81. Illumina microarray data was analyzed using Lumi on the log2 scale and was analyzed using the empirical Bayesian method implemented in Limma. Gene expression was analyzed using a t-test between cancer and WT mice or between tumor and normal adjacent tissue in patients. Transcripts with a *p*-value of less than 0.05 were considered to be differentially expressed. Benjamini-Hochberg false discovery rates were included.

Metabolomics

Metabolomics was performed using a platform that incorporates two separate ultrahigh-performance liquid chromatography/tandem mass spectrometry (UHPLC/MS/MS2) injections and one gas chromatography/mass spectrometry (GC/MS) injection per sample by Metabolon (USA). Identification, relative quantification, data-reduction and quality-assurance components of the process were

included in the analysis platform. 343 metabolites were identified (Data S3). The informatics system consisted of four major components, the Laboratory Information Management System (LIMS), the data extraction and peak-identification software, data processing tools for QC and compound identification, and a collection of information interpretation and visualization tools for use by data analysts. The hardware and software foundations for these informatics components were the LAN backbone, and a database server running Oracle 10.2.0.1 Enterprise Edition. For more details, see description of Metabolon QC samples in Table S15.

Real-time PCR

Total RNA was isolated and purified using an Ultra-Turrax rotating-knife homogenizer and the mirVana miRNA Isolation Kit (AM1560, Ambion) according to the manufacturer's instructions. Mouse WNT pathway RT2 profiler PCR array was used (StepOnePlusTM, Applied Biosystems), which targeted key genes involved in the canonical and non-canonical WNT pathway and endogenous genes for reaction control (89 genes and 7 controls, see Table S1). The reaction was performed according to the manufacturer's instructions (SABiosciences Corporation, QIAGEN Norway).

Data visualization

R/Bioconductor environment was used to process omics-data before differential expression analysis. Graphical data visualization and data analyses were carried out using GraphPad Prism software 6.0 (GraphPad Software, U.S), Excel 2016 (Microsoft), IPA (Qiagen, Aarhus, Denmark) and RStudio version 3.5.2 (2018-12-20). Diagram plots in Figure 5 were created with JavaScript library D3.js v.4. SPSS v.23-25 was used to perform test statistics including *t*-tests and non-parametric tests, one-way ANOVA, and correlation/linear regression analyses. Heatmaps were encoded in RStudio using the heatmap.2 function. Single-cell data were processed using Seurat v3 (doi.org/10.1016/j.cell.2019.05.031) and visualized in a tSNE plot (Figure 3). IPA was used to cluster cell-specific marker genes to WNT/mTOR-glutamine-dependent gene markers in Figures 8C-D and Figures S6A-E.

Ingenuity Pathway Analysis (IPA)

Transcriptomics and metabolomics datasets were analyzed using IPA (Qiagen, Hilden, Germany) which has sophisticated algorithms and criteria to calculate predicted functional activation/inhibition of canonical pathways, diseases and functions, transcription regulators and regulators based on their downstream molecule expressions (QIAGEN Inc., https://www.qiagenbioinformatics.com/products/ingenuitypathway-analysis). For human GC microarray, Illumina identifiers (ILMN) were uploaded together with log_2-fold change, *p*-values and *q*-values (false discovery rates). A total of 47,323 transcripts was assigned to analysis. A total of 37,489 transcripts were mapped/9,834 transcripts unmapped by IPA. For RNA sequencing, Ensembl identifiers were uploaded together with log_2-fold change, *p*-values and q-values. A total of 54,460 transcripts was assigned to analysis. A total of 53,735 was mapped/725 unmapped by IPA. For mouse GC microarray, ILMN were aligned together with log_2-FC and q-values before

uploaded in IPA. A total of 12,519 transcripts was loaded, a total of 11,773 transcripts was mapped/746 unmapped in IPA. For metabolomics, HMDB and KEGG identities were aligned together with fold changes, expressed *p*-values and *q*-values. A total of 343 metabolites were uploaded for downstream analysis in IPA and 252 metabolites were mapped by IPAThe data was subjected to a metabolomics expression analysis using HMDB or KEGG as identifier type. One-way ANOVA was used between groups. Fold changes were inverted before IPA analyzes. Thus, a molecule with 0.5-fold change was negatively inverted (-1/0.5) to -2.0.

Regulatory z-scores for canonical pathways that overlapped with our experimental data were calculated using the formula described previously (Krämer et al., 2014). To generate the network of up- or down-regulated genes, custom-made molecular networks were developed based on information contained in the IPAs knowledge base. Networks of these genes were then algorithmically generated based on their interrelationships. Filtering of datasets included species, *p*-value cut-off and/or *q*-value cut-offs. Molecular networks and canonical pathways were algorithmically constructed based on known connectivity and relationships among metabolites and genes/proteins using IPAs knowledge base. The significance of the association between the dataset molecules and the canonical pathways was measured by Fischer's exact test that was used to calculate a *p*-value determining the probability that the association between the genes in the dataset and the canonical pathway by chance alone. Z-scores were calculated in IPA based on the dataset's correlation with the activated state. Negative z-scores indicate a decrease in activity, positive z-scores indicate an increase in activity. Canonical pathways were identified using statistical cut-offs at $p<0.05$ and/or $q<0.05$.

In silico experiment

Signaling pathways of WNT/β-catenin and mTOR were constructed based on the transcriptomic data of INS-GAS mice and were then entered into the "Pathway" module of the IPA to obtain the nodes in every corresponding signaling pathway. The expression data from INS-GAS *vs.* FVB mice (Mouse GC *vs.* WT) was compared to all genes in the pathways. Nodes were added as entries into the "My list"-function and all entries in the list were added to the "My pathway" in IPA. My pathway was used to produce a network of nodes/genes from the WNT and mTOR signaling pathways that matched with our experimental data from INS-GAS *vs.* FVB. The build-tool was used to connect nodes using edges, i.e. relationships including both direct and indirect interactions like chemical-protein interactions, ubiquitination, molecular cleavage, translocation, localization, phosphorylation, expression, protein-protein interactions, activation, regulation of binding, inhibition, membership, reaction, protein-DNA interactions, transcription and modification. The Canonical Pathway overlay-tool was used to arrange the entries into two clusters based on pathway. Next, the molecule activity predictor (MAP)-function was used to predict activation/inhibition between the nodes in the network. The *in silico* tool was employed to predict effects on the network after gene inhibition. Categorical values were set to each gene/node using a semi-quantitative method to quantify the color-change resulting from *in silico* inhibition. Dark blue colored nodes were represented by -2, light blue as -1, white as 0, light orange

as +1 and dark orange as +2. Values are represented of n=7-14 experiments per inhibition node/gene.

Upstream regulator analysis

Ingenuity pathway analysis (IPA, QIAGEN) was used to perform upstream analysis of the transcriptomics datasets based on the literature and the Ingenuity Knowledge Base. The analysis examines how many known targets of the upstream regulators are present in the dataset. An overlap *p*-value is computed based on significant overlap between genes in the dataset and known targets regulated by the transcriptional regulator. The activation z-score algorithm is used to make predictions. In mouse GC, 144 regulators were found to be activated (z-score>2, $p<0.05$) based on the expression levels of target molecules in the datasets. The overlay-tool in the "My pathway" module was used to cluster the activated regulators into canonical pathways. Next, upstream regulators of interest were added into custom-made pathways in the Path Designer-tool and relationship-types between upstream regulator and target molecule were added.

tSNE plot of metabolic gene expression according to single-cell atlas

Available data on a single-cell transcriptome network of gastric premalignant and early gastric cancer in patients was utilized (PMID: 31067475), including 13 biopsies from 9 patients: 3 mild superficial gastritis (NAG), 3 chronic atrophic gastritis (CAG), 6 intestinal metaplasia (IM), and 1 early gastric cancer (EGC). Single-cell data were processed using Seurat v3 (doi.org/10.1016/j.cell.2019.05.031) and normalized for each of the 13 samples independently. The functions FindIntegrationAnchors, IntegrateData, ScaleData and RunPCA with default parameters were used. Cells with number of expressed genes lower than 400 or larger than 7000 and 20% or more of UMIs mapped to mitochondrial or ribosomal genes were removed. 50 PCs were utilized to visualize single-cell atlas with a tSNE plot. The expression levels of marker genes in mouse GC *vs.* WT for each representative cell type were analyzed. Marker genes were identified by differential expression analysis with the threshold as fold change > 1.5 and FDR < 0.01.

Statistics

Values are expressed as means ± SEM or SD and statistical methods are shown in the figure legends.

Supplemental references

Ianevski, A., Giri, A. K., Gautam, P., Kononov, A., Potdar, S., Saarela, J., Wennerberg, K. & Aittokallio, T. (2019). Prediction of drug combination effects with a minimal set of experiments. Nature Machine Intelligence *1*, 568-577.

Ianevski, A., He, L., Aittokallio, T. & Tang, J. (2017). SynergyFinder: a web application for analyzing drug combination dose–response matrix data. Bioinformatics *33*, 2413-2415.

Krämer, A., Green, J., Pollard, J., Jr. & Tugendreich, S. (2014). Causal analysis approaches in Ingenuity Pathway Analysis. Bioinformatics (Oxford, England) *30*, 523-530.

Wang, T. C., Koh, T. J., Varro, A., Cahill, R. J., Dangler, C. A., Fox, J. G. & Dockray, G. J. (1996). Processing and proliferative effects of human progastrin in transgenic mice. J Clin Invest *98*, 1918-29.

Zhang, P., Yang, M., Zhang, Y., Xiao, S., Lai, X., Tan, A., Du, S. & Li, S. (2019). Dissecting the Single-Cell Transcriptome Network Underlying Gastric Premalignant Lesions and Early Gastric Cancer. Cell Rep *27*, 1934-1947 e5.

Zhao, C. M., Hayakawa, Y., Kodama, Y., Muthupalani, S., Westphalen, C. B., Andersen, G. T., Flatberg, A., Johannessen, H., Friedman, R. A., Renz, B. W., et al. (2014). Denervation suppresses gastric tumorigenesis. Sci Transl Med *6*, 250ra115.